Comparison between economic growth and satellite-based measurements of NO₂ pollution over northern Italy

Renée Bichler [a,b,*], Michael Bittner [a,b]

[a] German Remote Sensing Data Center, German Aerospace Center, Oberpfaffenhofen, Germany
[b] Institute of Physics, University of Augsburg, Augsburg, Germany

HIGHLIGHTS

- Long-term time series analyzes of tropospheric NO₂ total column of the Po valley.
- Using spectral analysis methods such as harmonic and wavelet analysis.
- Comparison of economic fluctuations (GDP development) and the NO₂ variability.
- A significant decrease in NO₂ variability fitted strikingly well with the global economic crisis.

ABSTRACT

The aim of this study is to investigate to what extent spatiotemporal fluctuations in the tropospheric NO₂ column concentration can map variations in economic output. To do so satellite based tropospheric NO₂ column measurements obtained from the ERS-2, ENVISAT, MetOp-A, and MetOp-B satellite missions covering the period from 1996 to 2017 over the Po valley in northern Italy is analyzed. A harmonic analysis is carried out in order to exclude influences such as the annual or semi-annual cycle. Afterwards the residues of the tropospheric NO₂ time series are further investigated by means of a wavelet analysis method. The result is a spectrogram which implies the NO₂ variability for the study area between 1996 and 2017. Therefore, the gross domestic product (GDP) is used as an indicator for economic performance and thus, as an approximation, of anthropogenically induced NO₂ pollution. Clear conspicuous signatures occurred almost simultaneously both within the temporal development of the GDP growth rate and the spectral characteristic of the NO₂ variability during the studied period. The comparison of the temporal course of the GDP shows that the period of systematically reduced spectral intensity in NO₂ coincides strikingly well with the period of the global financial crisis in 2008 which was then followed by a second crisis in 2014. The economic growth decreased by 7.9% between 2007 and 2009 and by 5.2% between 2011 and 2014 in comparison to the same quarter of the previous year. It is found that during the crises (2007–2013) the variability of NO₂ is reduced by about 80%.

1. Introduction

Satellite based measurements provide the opportunity to collect air pollution data on a global scale, self-consistent and according to a uniform quality standard, as well as with a mostly daily coverage. One of the most important pollutants is nitrogen dioxide (NO₂) which affects human health, ecosystems, and is an important precursor to ozone (O₃), itself a prominent air pollutant. Together with nitrogen monoxide (NO) it refers to nitrogen oxides, NO$_x$ = NO + NO₂ (see for example Seinfeld and Pandis, 2016, for a comprehensive overview). Main sources for NO$_x$

are on the one hand anthropogenic causes like fossil fuel combustion and biomass burning. On the other hand, natural causes such as lightning or injection of air masses from the stratosphere into the troposphere. NO$_x$ is – like ozone (O₃) – a comparatively long-lived species in the lower stratosphere having its origin in the middle tropospheric stratosphere (Brasseur and Solomon, 1986). As NO₂ is a highly reactive trace gas which has its principle sink during daytime when the gas reacts with hydroxyl (OH) (see for example Wallace and Hobbs, 2006, for a more detailed description), the lifetime of NO₂ in middle latitudes typically varies between some hours (during summer) up to one day (during

winter) near the ground. The lifetime increases with height reaching up to even a few days near the tropopause (Levy II et al., 1999). Shah et al. (2020), pointed out that the seasonal lifetime difference of NO_2 make it difficult to estimate trends from satellite-based measurements of the tropospheric column.

Regarding NO_2 investigations in northern Italy, several studies can be referenced. Bigi et al. (2012) for example analyzed hourly data for carbon monoxide (CO), NO, NO_2, NOx, and O3 as well as daily particulate matter $< 10\mu m$ (PM10) with a long-term time series from 1998 to 2010 for an urban background station in Modena, Emilia-Romagna, northern Italy. The authors studied furthermore the yearly, seasonal, weekly, and diurnal variations of the pollutants in the Po valley. They concluded that NO_2 shows a strong traffic-related pattern especially during morning and evening rush hours as well as lower pollution on weekends. Masiol et al. (2014) also examined hourly air pollution data for various pollutants (in total 13) including NO_2 with a long-term time series from 2000 to 2013 in the eastern part of the Po valley for an urban background site in Mestre-Venice. The research was done to better understand vehicle emissions also regarding to adopted measures in cities such as car-free days for example. Additionally, Degraeuwe et al. (2017) focused on the urban NO_2 pollution for street canyons in eight different European cities containing Milan in northern Italy. Another publication by Bo et al. (2020) reports about a citizen science campaign in Torino in the western part of the Po valley. The focus of this project was the public engagement by measuring NO_2 pollution in the megacity region. Due to the fact that the Po valley is because of its orography an area where pollutants accumulate quite well the publication by Raffaelli et al. (2020) should be mentioned here as well. In their study the impact of current air pollution measures (2013) and further investigations (2025) are analyzed within a project called LIFE-IP-PREPAIR (EU LIFE-IP Clean Air Program Po Regions Engaged to Policies and Air).

Using satellite-based data, several studies were performed to study the relation between pollutants and economic development such as Castellanos and Boersma (2012) as well as Russell et al. (2012). Castellanos and Boersma (2012) investigated the tropospheric NO_2 column density measured by OMI on board of the Aura satellite between 2004 and 2010 over Europe. They concluded that environmental policy measures led to a 10%–50% reduction of NO_2 between 2004 and 2010. The authors mentioned that relative to concentrations in 2004, the global economic crisis in 2008 contributed to a NO_2 decline in Europe of 15%–30% in the year 2009. Russell et al. (2012) analyzed the effects of emission control technology as well as the impacts of the global economic recession during 2008 by also using Aura/OMI NO_2 measurements for the United States (US). They observed an average change of NO_2 pollution of $-32 \pm 7\%$ between 2005 and 2011 over urban areas in the US. The authors concluded that these emission reductions can be ascribed to successful improved emission control technologies for on-road mobile emission sources. They examined three different periods between 2005 and 2011 to analyze the impacts of the economic recession. The authors thus studied the NO_2 tropospheric column density over US cities before (2005–2007), during (2007–2009), and after (2009–2011) the global economic crisis. The results show declining NO_2 emissions of $-6 \pm 5\%$ before, $-8 \pm 5\%$ during, and $-3 \pm 4\%$ after the crisis.

Moreover, 2020 presented the world with ones of its greatest challenges in the recent decades. The coronavirus, also known as SARS-CoV-2 or COVID-19, caused a pandemic that put the entire world into an economic and social emergency. Significant restrictions were imposed on populations at a global scale which has shown the anthropogenic influence on our environment. For instance, Le Quéré et al. (2020) reports on the temporary reduction in daily CO2 emissions during the COVID-19 lockdown while Steinbrecht et al. (2021) address the impact of the pandemic on the reduction of free tropospheric ozone across the Northern Hemisphere.

Filonchyk et al. (2020) analyzed the lockdown effect on air pollution in Shanghai and the Yangtze River Delta. China's strict containment and isolation policies significantly reduced economic activity from which the authors were able to calculate a particulate matter $< 2.5\mu m$ (PM2.5) reduction of 9%, PM10 of 77%, sulphur dioxide (SO2) of 31.3%, NO_2 of 60.4%, and CO of 3%. Another similar research by Filonchyk et al. (2021) on the impact of the COVID-19 pandemic and air pollution in Poland presents findings based on satellite data. The drastic decline in economic activities, as well as the limitations on individual mobility, led to a general decrease in the range of 47.9% (during the lockdown) to 20.3% (after the lockdown) in aerosol optical depth (AOD). An overall reduction of 10.8% in NO_2 and 25.6% in SO2 was observed when comparing satellite measurements from 2020 with those of 2019 for the same period. On a global scale, Liu et al. (2021) analyzed the COVID-19 lockdown effect on NO_2 pollution based on GOME-2 and TROPOMI measurement data for selected cities in Asia, Europe, North America, and South America. The NO_2 reductions were on average in the range of 30%–50%. Further studies of the relationship between economic growth and the possible impact on the environment were done by Grossmann and Krueger (1995), Dinda et al. (2000), and Jiang et al. (2020).

The range of the economic impact on air pollution scopes from energy production, industrial processes, traffic, and agriculture. The question of how economic growth affects the environment is complex, and as far as we know, still far from being fully understood. The goal of our study is to quantify the possible impact of fluctuations in economic productivity on the spatiotemporal variability of the tropospheric NO_2 column density instead of the absolute values of the tropospheric NO_2 column density. To do so we analyzed the tropospheric NO_2 column densities measured by satellites by means of a wavelet analysis and compared the NO_2 variability with the gross domestic product, GDP, for northern Italy in the period between 1996 and 2017. The overall question to which this study will contribute is whether it is possible to develop a response function that can relate GDP variation to air pollution. It is of interest to study and quantify the extent to which the respective level of economic development plays a role in this context. If successful, satellite-based measurements of air pollutants could add value to global monitoring of economic development.

The paper is organized as follows: the data we used are described in section 2. Preparation of data and data analysis techniques to especially derive spectral information from the time series and results are presented in section 3. Results are given in section 4 while section 5 is concerned with the discussion and interpretation of the results. The main findings and an outlook to future work are summarized in section 6.

2. Data

2.1. Tropospheric NO_2 total column concentration

Industrial plants, traffic routes, and densely populated areas are among the most prominent sources of NO_2. Due to its comparatively short lifetime and due to the influence of weather conditions (wind, precipitation, temperature), the concentration of NO_2 may vary considerably in space and time. It therefore becomes clear that the limited number of ground-based NO_2 monitoring stations cannot always capture this variability. This is where satellite-based measurements can add value as they provide area-wide self-consistent measurements at a global scale. However, the satellite-based measurements used in this study are nearly always taken at the same local time of the day (see Table 1) over northern Italy. As such, they do not provide NO_2 concentrations at the surface level *per se*. Rather, a so-called total column density is observed. This is understood as the number of NO_2 molecules in a vertical column of air within a unit area from the ground up to the satellite. The proportion of NO_2 molecules in the troposphere in the total column can then be estimated from these measurements (see for example Boersma et al., 2017). Recalling the limited life-time of the ground-level NO_2 we use the so-called "tropospheric NO_2 column density" in our study as an area-wide average proxy of NO_2 pollution near

Table 1

Overview about the satellites and respective measurement instruments for the tropospheric NO_2 column density. Data of instruments indicated in grey shading are not used for further analysis (details see text).

Satellite	Instrument	Mission	CET	deg. regl. Grid
Sentinel-5P	TROPOMI	2018-tody	13:30 asc	0.125×0.125
Aura	OMI	2004-today	13:45 asc	0.125×0.125
MetOp-B	GOME-2B	2013-today	09:30 desc	0.25×0.25
MetOp-A	GOME-2A	2007-today	09:30 desc	0.25×0.25
Envisat	SCIAMACHY	2002–2012	10:00 desc	0.25×0.25
ERS-2	GOME	1996–2003	10:30 desc	0.25×0.25

the ground. More precisely, we assume that the temporal variation of the tropospheric NO_2 column density can – within certain limitations – be considered as an indicator for the temporal variability of the ground-level NO_2 concentration.

Our analysis is based on the tropospheric NO_2 column density measured by MetOp-A/GOME-2A, MetOp-B/GOME-2B, Envisat/SCIA-MACHY, and ERS-2/GOME over a period from 1996 to 2017. Overviews on these instruments are given by Burrows et al. (1999) (GOME), Burrows et al. (1995), and Bovensmann et al. (1999) (SCIAMACHY) and Munro et al. (2016) (GOME-2). Information about the observation periods and equatorial crossing times is given in Table 1. As the use of time series obtained from different sensors is always delicate, we do not use the individual data series for our study. Instead the harmonized self-consistent global data product compiled by Georgoulias et al. (2019) which includes all four satellite measurements was used. The product is provided by TEMIS (www.temis.nl).

Detailed information of the merged TEMIS data product which covers the period from 1996 to 2017 is given by Georgoulias et al. (2019). Additional information about the TEMIS product can further be found in Boersma et al. (2004).

Note that NO_2 observations from aboard the US Aura satellite (instrument OMI) and the European Sentinel-5P satellite (instrument TROPOMI) were also active during the time period studied here. However, the overpass times for these systems above northern Italy deviate comparatively strongly from those of the other systems listed in Table 1. The instruments GOME, SCIAMACHY, and GOME-2A/B provide measurements over the study area between 09:30 and 10:30 in the morning (CET). OMI and TROPOMI each measure between 13:30 and 13:45 (CET) early in the afternoon. This is significant for our study because the tropospheric column density of NO_2 is well-known to be subject to a pronounced diurnal cycle especially in mid-latitudes. For example, Velders et al. (2001), based on comparisons with models, show that the ratio of tropospheric NO_2 column density at about 10:30 CET (they used GOME data) and the daily mean of tropospheric NO_2 column density (estimated with the IMAGES model) for the observation area used in this study can be as high as 50–60%. This would strongly affect our analyses and we have therefore excluded data taken by TROPOMI and OMI.

For our studies the merged TEMIS monthly mean data product is used on a standard grid of $0.25° \times 0.25°$ and the observations were averaged monthly. As cloud cover limits satellite-based measurements of tropospheric NO_2 (Boersma, 2008) the TEMIS data only considered measurements with a cloud radiance fraction less than 50% which is equivalent to a cloud fraction of around $<20\%$ to reduce cloud cover effects. The data is generated by gridding the data and referring to Boersma (2008) this can also lead to different pixel overlapping statistics.

Even though the TEMIS data product is based only on satellite measurements that were collected when cloud cover was low, a data quality check was conducted with regard to cloud cover by using the total cloud cover for the same study area from the European Center for Medium-Range Weather Forecast (ECMWF) reanalysis version 5 (ERA5) dataset (Hersbach et al., 2018). Heavy cloud cover naturally affects the observations and thus can have an impact on our analysis of the temporal tropospheric NO_2 column density fluctuations. To cross-check the consistency of the data, we looked at the daily total cloud cover for northern Italy on the basis of ERA5 data between 08:00 and 10:00 UTC (overpass times of the satellites) and for the period 1996 to 2021.

Fig. 1 represents the number of days per month with a total cloud cover less than or equal 20%. The spline (blue curve) indicates that on average eight days per month are available with a total cloud cover of less than 20%. During winter, the total cloud cover intensifies as seen in Fig. 1 representing the daily total cloud cover from 1996 to 2021 separated by each month (violin plot with the included boxplot). The grey shaded body of the violin plot provides information about the distribution of the data. It can be seen that the shape of the violin evolves due to seasonal changes. Fig. 1 also includes a boxplot which provides information about the mean values (red points), the median (horizontal marking), as well as the 25th and 75th percentiles, minimum, and maximum outliers. From October to January, the median reaches its highest values due to many days with a very high total cloud cover and less days with low total cloud cover. During this period, it is also visible that the median deviates more from the mean value. Overall, the cloud cover in the period studied is about 50% on average (not shown here). We therefore support that the time series of the monthly averaged tropospheric NO_2 column density represents a reliable data source for our analyses.

The target area in our study is northern Italy because of its geographical characteristics and its share of Italy's GDP. The area in the north and west of Italy is dominated by the Alps and includes the northern Italian lowlands (Po valley). This area of interest is shown in Fig. 2. The Alps in the north/west and the Apennines in the south act as a barrier for air flows. Consequently, NO_2 often accumulates in the Po valley.

As a typical example for such a situation, Fig. 3 shows the spatial distribution of NO_2 column density as a monthly average for January 2020 over this area, measured by the GOME-2B instrument on board of the MetOp-B satellite. It is worth reminding that the data are always taken at nearly the same local time of the day. The chosen study area is highlighted with a red rectangle. The NO_2 pollution around the cities such as Milan and Turin or the area around Bergamo, Brescia, Verona, and Venice are clearly noticeable as they are mostly located within the red and orange areas.

2.2. Italian GDP

The largest contribution to GDP in Italy comes from the northern region where most its industries are located (see, for example, the G-Econ Project, 2009). Italy's GDP is essentially determined by agriculture (so-called 'primary sector'), industry and manufacturing ('secondary sector'), as well as the service sector ('tertiary sector'). The service sector clearly dominates, accounting for up to 60% of GDP. In second place are industry and manufacturing with a combined share of about 40% of GDP. The contribution from agriculture, on the other hand, is comparatively small. Fig. 4 presents the temporal development of the sectoral distribution of the GDP for Italy between 1996 and 2019. Data is provided by the World Bank (2020).

The temporal development of the Italian GDP from 1997 to 2020 for several European countries is given in Fig. 5. Italy's economy grew overall in the period up to around 2008. The same applies to the other European countries in Fig. 5. The increase in this phase is superimposed by minor to moderate fluctuations. The global financial crisis that began in 2007/08 disrupted Italy's economy, from which the country did not initially recover. There was a massive decline in economic output of up to 8%. After a short period of economic recovery, Italy was again confronted with a strong decrease of the GDP between 2011 and 2014 of around 5%. Then, from 2014 onward, a continuous increase is observed albeit lagging behind other countries showcased in Fig. 5. More recently, in 2020, northern Italy was one of the hardest hit areas in the world due to the COVID-19 pandemic.
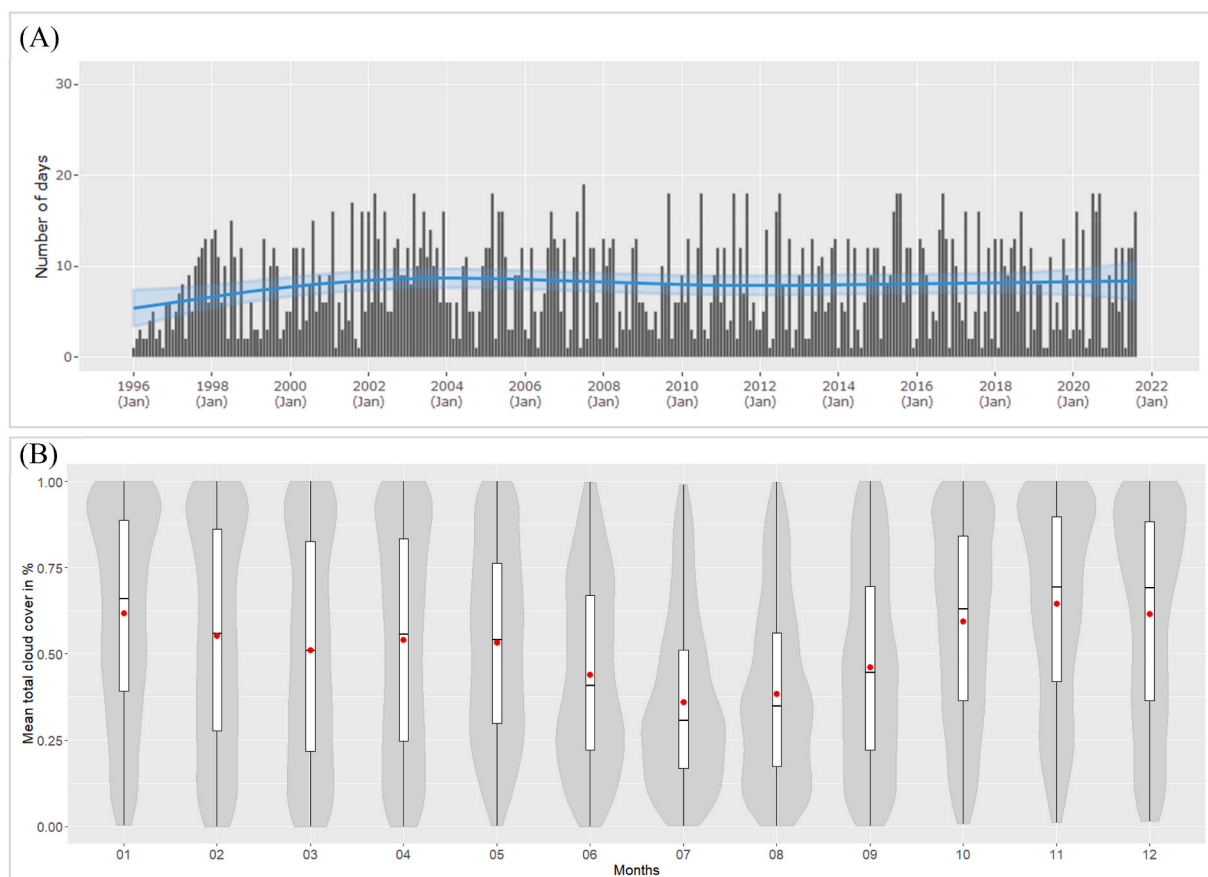
Fig. 1. (A) Available number of days with a total cloud cover of less than 20% for the period 1996–2021 for northern Italy; Blue line represents a cubic spline, (B) Violin plot with included boxplot; Data shows the ERA5 daily total cloud cover for the period from 1996 to 2021 for northern Italy; Red dots represent the mean value and the horizontal lines emphasizes the median (Hersbach et al., 2018). (For interpretation of the references to colour in this figure legend, the reader is referred to the Web version of this article.)

2.3. Meteorological data

In order to examine the possible meteorological influences, the ERA5 data from the Copernicus Climate Change Service (C3S) was used. For this purpose, a monthly mean time series of the total precipitation and the 10 m wind (zonal wind u, meridional wind v, and horizontal wind) from 1996 to 2021 was created for the area of interest. To ensure that the temporal resolution of the model data matches the overflight times of the satellites, the mean value was calculated between 08:00 h, and 10:00 h (UTC). More information about the data set can be found in Hersbach et al. (2018).

3. Methods

3.1. Harmonic analysis

The method of harmonic analysis is a well-established spectral analytical approach and shall therefore only briefly be outlined. It makes use of the concept that discrete data series $y(t)$, $t = 1,\ldots N$ can be represented - up to a certain degree - by a suitable linear combination of n trigonometric functions. If the parameters of the n trigonometric functions (amplitude A_i, period τ_i, phase φ_i with $i = 1,\ldots n$) are known, the original discrete data $y(t)$ can be modeled by $y_{mod}(t)$ based on the least square's technique, see equations (1) and (2). Note that the discrete data series does not have to be equidistant (e.g. data gaps are allowed within an evenly spaced data series).

$$y_{mod}(t) = \sum_{i=1}^{n} A_i \cdot sin\left(\frac{2\pi}{\tau_i} t + \varphi_i\right) \tag{1}$$

$$\sum_{t=1}^{N} [y(t) - y_{mod}(t)]^2 \to 0 \tag{2}$$

We use this technique to adjust the tropospheric NO_2 column density data series for seasonal variations (e.g. annual and semi-annual variations). The technique allows to first fit a sine function to the data series and then to subtract it from the data. Another sine function can then be fitted to the residuals, and so on (see equation (1)). The resulting linear combination of sinusoidal functions often turns out to be non-unimodal, i.e. the variance of the data series can be further reduced by simultaneously re-optimizing the previously determined parameters (phase and amplitude of the previously determined sinusoidal functions) at each step. These optimization aspects are described in more detail in Bittner et al. (1994). In order to solve the associated convergence problems within acceptable computation times, the Newton-Raphson method is used to solve the nonlinear system of equations (see e.g. Ortega and Rheinboldt, 1970).

3.2. Wavelet analysis

The wavelet analysis is a well-established method to examine time series for possible periodic or quasi-periodic signals. The particular advantage of this method is that the examined time series do not necessarily have to show stationarity in the statistical sense. In other words, they do not require the same statistical moments (in particular
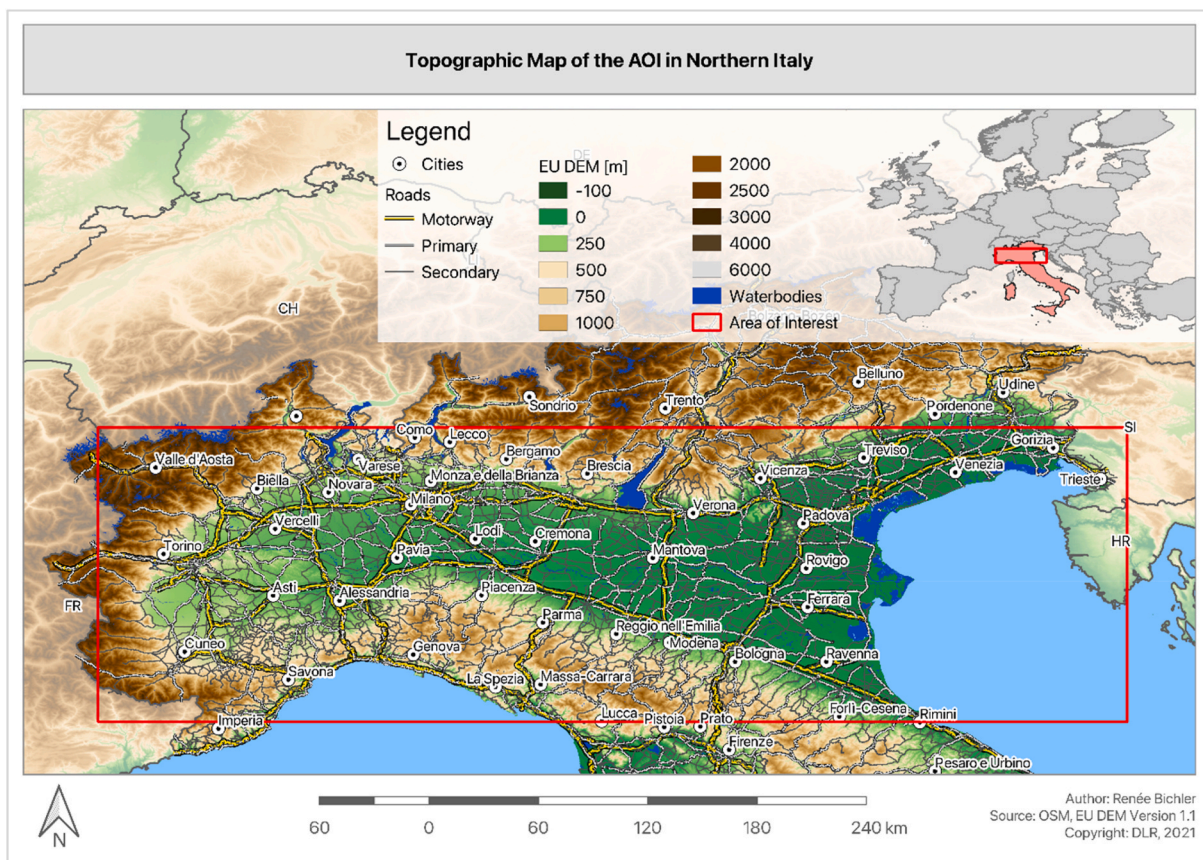
Fig. 2. Topographic map of the area of interest in northern Italy, Po valley. (Source: OSM and EU Digital Elevation Model (DEM) version 1.1).
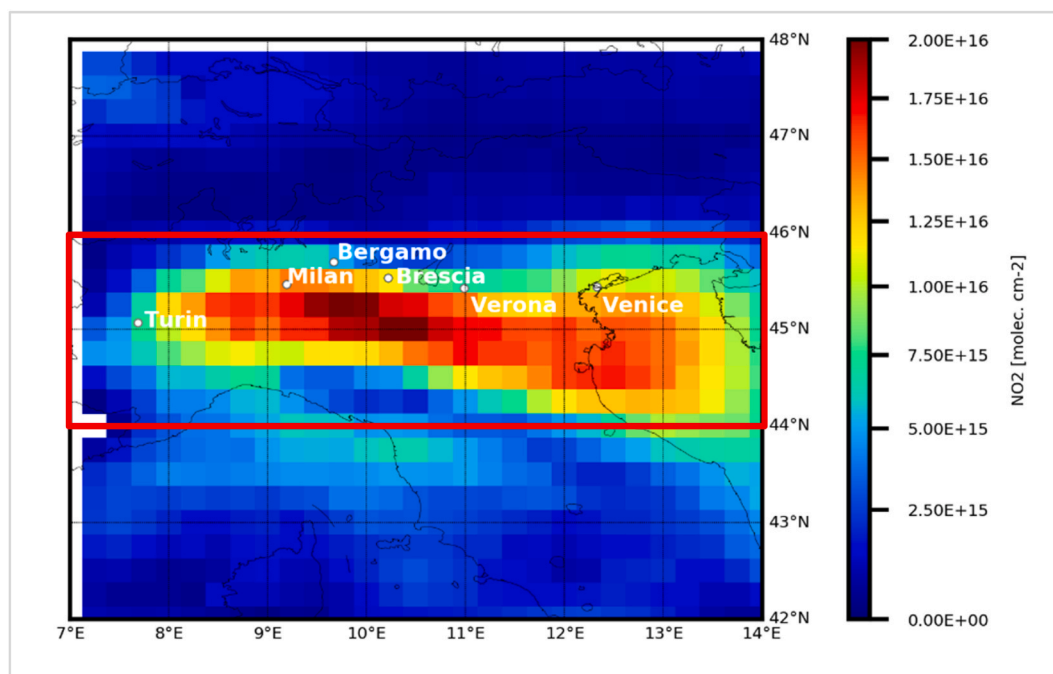

Fig. 3. NO_2 distribution in January 2020 in northern Italy measured by the GOME-2B instrument on board of MetOp-B satellite. Data are provided by TEMIS (www. temis.nl).

mean value and standard deviation) at all times. It can be shown that this circumstance can also be expressed in such a way that the periodic signals possibly contained in the time series need not always have the same amplitude and period over the entire time series, or need not be present all the time at all. Indeed, the time series of NO_2 distribution and GDP examined in this study turn out to be non-stationary. Wavelet
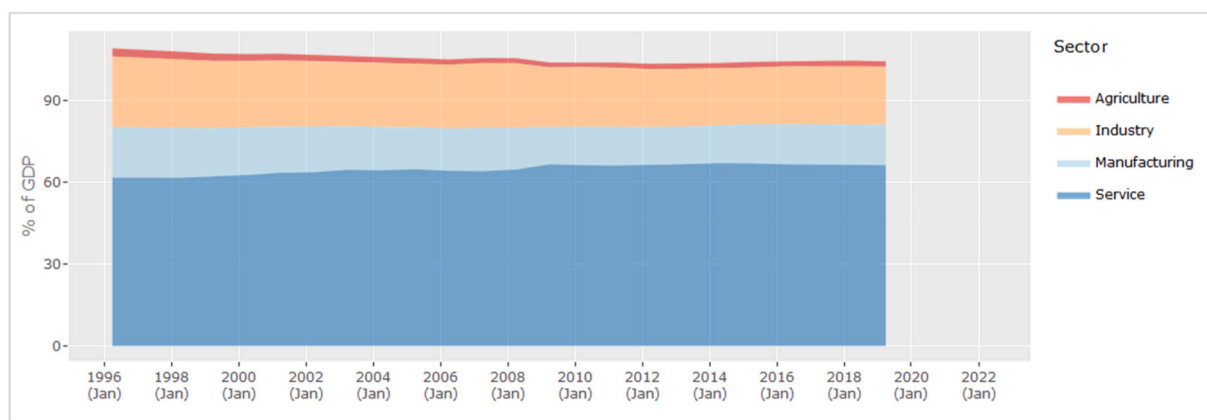
Fig. 4. World Development Indicators: Structure of output for Italy (World Bank, 2020).
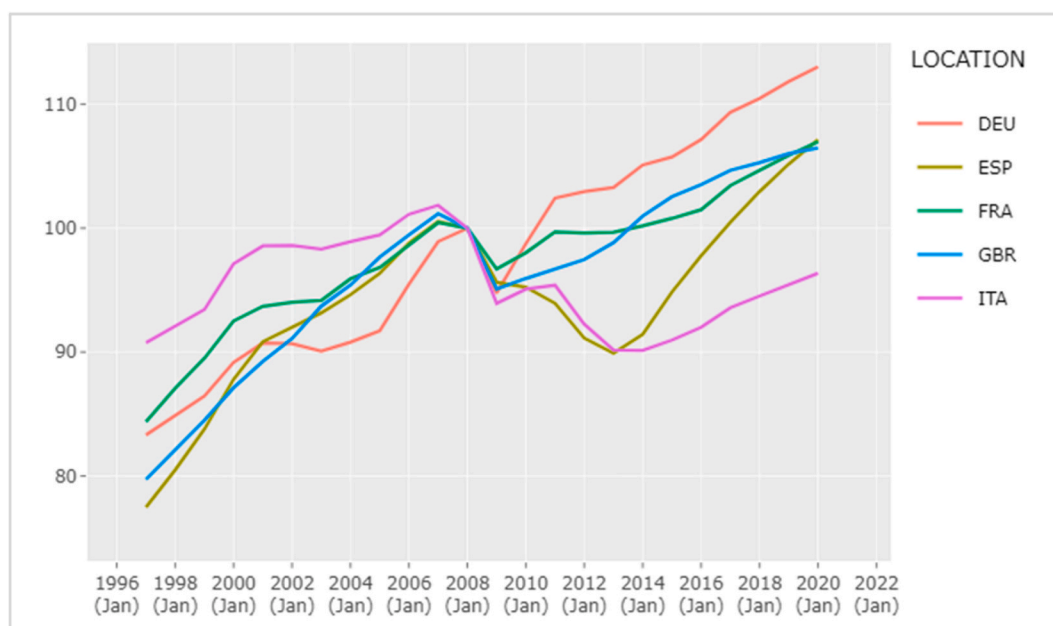

Fig. 5. Temporal development of the real GDP per capita for different European countries (Germany (DEU), Spain (ESP), France (FRA), Great Britain (GBR), Italy (ITA)) from 1997 to 2020 with the reference year set at 2008; Calculations are based on the OECD "Gross domestic product per capita, volume in USD, at constant purchasing power parities" (GDPVD_CAP) data table (OECD, 2021).

analysis has often proven to be a robust and suitable tool in such cases. It provides a locally resolved spectrum and does not average the spectral characteristics of the whole data series. We will not go into more detail here since the analysis technique is already described in earlier work such as Wuest and Bittner (2006) and Bittner et al. (2000). Reference is also made to Torrence and Compo (1998) and Chui (1992) to mention just a few. The following are just a small amount of the key aspects.

$$s(a,b) = \frac{1}{\sqrt{a}} \int_{-\infty}^{\infty} f(t) \, h\left[\frac{t-b}{a}\right] dt \qquad (3)$$

The wavelet transform is given by the equation.where $f(t)$ represents the time series. h represents the so-called basic wavelet. a is the dilation-scale factor and determines the characteristic frequency while b represents the translation in time. The wavelet h used in this work is the *Morlet* wavelet. It is given by

$$h(t) = \frac{1}{\pi^{[1/4]}} \left[e^{ikt} - e^{-k^2/2} \right] e^{-t^2/2} \qquad (4)$$

where

$$k = \pi \left[\frac{2}{\ln 2} \right]^{1/2} \qquad (5)$$

To generate a wavelet analysis in this study we applied to the data the "WaveletComp R″ package from Roesch and Schmidbauer (2018).

4. Results

4.1. NO$_2$ long-term trend

As mentioned in section 2, Georgoulias et al. (2019) compiled a global tropospheric NO$_2$ column density data product by using data from the GOME, SCIAMACHY, GOME-2A, and GOME-2B instruments which we also use here. The satellite of GOME and GOME-2 has been adapted to the measurements of SCIAMACHY which made it possible to create a self-consistent dataset for the period 1996 to 2017. Based on this tropospheric NO$_2$ satellite product the study area of northern Italy (44° N to 46° N and 7° E to 14° E) could be generated.

The tropospheric NO$_2$ time series is characterized by a long-term

decreasing trend. To quantify this, a cubic least squares spline was fitted to the data series (blue curve in Fig. 6). The decrease is quasi-linear to a good approximation and can be estimated of about $3.14 \cdot 10^{15}$ *molec.* cm^{-2} from 1996 to 2017.

4.2. NO_2 - seasonal and sub-seasonal variability

Fig. 6 clearly reveals that an annual variation with systematically higher values during winter and lower values during summer is superimposed on the longer-term trend. The difference in tropospheric NO_2 column density is on average in the order of about $1 \cdot 10^{16}$ *molec.cm*$^{-2}$ between summer and winter. It should also be noted that the summer minima are apparently somewhat broader in terms of time than the winter maxima. It is also noticeable that the amplitude of the annual cycle can vary considerably from year to year.

The temporal variability of the tropospheric NO_2 column density is not limited to a long-term trend and the annual cycle. There are also variabilities on other time scales. To quantify these, we applied the wavelet analysis to the time series shown in Fig. 6. The corresponding spectrogram is shown in Fig. 7. As expected, the annual cycle clearly dominates the spectrogram. There is also evidence for a quasi-semi-annual oscillation. However, it is quite obvious that there is also variability in the tropospheric NO_2 column density with periods in the range of a few months. To better identify these shorter-period signals, we removed both, the annual and the semi-annual cycle from the NO_2 time series. Since the amplitude of the annual cycle varies from year to year, it was adjusted separately for each year in order to account for stationarity in a statistical sense by using the harmonic analysis approach (orange curve in Fig. 8; the original NO_2 time series presented in black). The blue curve in Fig. 8 presents the resulting time series of monthly NO_2 tropospheric column densities after taking out the annual and the semi-annual cycles and which was then again subjected to a wavelet analysis. The resulting spectrogram is shown in Fig. 8. Significant variability of the tropospheric NO_2 column density can be seen mainly in the range from about two to six months. It is noticeable that the spectral intensities are systematically increased over an extended spectral range during winter. Furthermore, it can be seen that the intensities are systematically lower in the range from about 2008 to mid-2013 than in the other years.

To better examine the short-term fluctuations, the mean value of the wavelet power intensity for each month and for the spectral range from two to six months was calculated based on the spectrogram shown in Fig. 8. While Fig. 9 illustrates the respective mean wavelet power values for each month, Fig. 9 likewise illustrates the mean values (red line) but also contains information about the standard deviation (grey bars) as well as the variance (black dots). Furthermore, both plots were split into three periods, period A (1999 to mid-2007), period B (mid-2007 to mid-

2013), and period C (mid-2013 to the end of 2016). A significant reduction in the NO_2 variability can be clearly seen during period B.

5. Discussion

5.1. NO_2 long-term trend

The long-term trend in tropospheric NO_2 column density estimated from 1996 until 2017 (see Fig. 6) for the greater Po valley area in northern Italy corresponds to a reduction of the tropospheric NO_2 column density by about 35% during this period. This number compares well with the findings reported by Georgoulias et al. (2019) which found a reduction of about 36% for Italy and with the results of Castellanos and Boersma (2012) for the tropospheric NO_2 column density through OMI measurements between 2004 and 2010 over Europe. In particular this value also agrees quite well with the trend estimates derived from ground-based station measurements that can – in contrast to satellite-based observations – actually measure the ground-level NO_2 concentration. For example, Fig. 10 shows the temporal development of ground-level NOx emissions from 1996 to 2018 for Italy as reported by the EEA (EEA, 2021 and EEAa, 2021). The reduction in NO_2 concentrations is largely attributed to the implementation of the national clean air plan (see EEA, 2021; Piersanti et al. 2021).

It should be noted that Schaap et al. (2013) calculated the expected relative emission change from 2005 to 2020 for all European countries. Based on this, Italy was expected to have a NO_2 emission reduction between 30 and 40% which also fits quite well with this study's findings.

5.2. NO_2 shorter term variability

The wavelet spectrograms (Figs. 7 and 8) of the temporal development of the tropospheric NO_2 column density over the area of northern Italy shows that NO_2 concentrations are subject to considerable temporal fluctuations over a wide scale ranging from a few months up to one year (and apparently beyond). The transient character of the tropospheric NO_2 column density time series in the statistical sense is clearly evident here. The fluctuations (apart from the annual and semi-annual oscillations) are not always present over the entire period from 1996 to 2017; the intensity of the fluctuations can vary significantly over time. The fluctuations must be the result of production and loss, as well as of transport of NO_2 and can be written as

$$\frac{\partial NO_2}{\partial t} = P_i - L_j - \vec{u}\vec{\nabla} NO_2 \qquad (6)$$

where t is time, $\vec{u}$ is velocity, $\vec{\nabla}$ is the three-dimensional spatial gradient operator. P denotes the production and L the loss of NO_2, i.e. the net
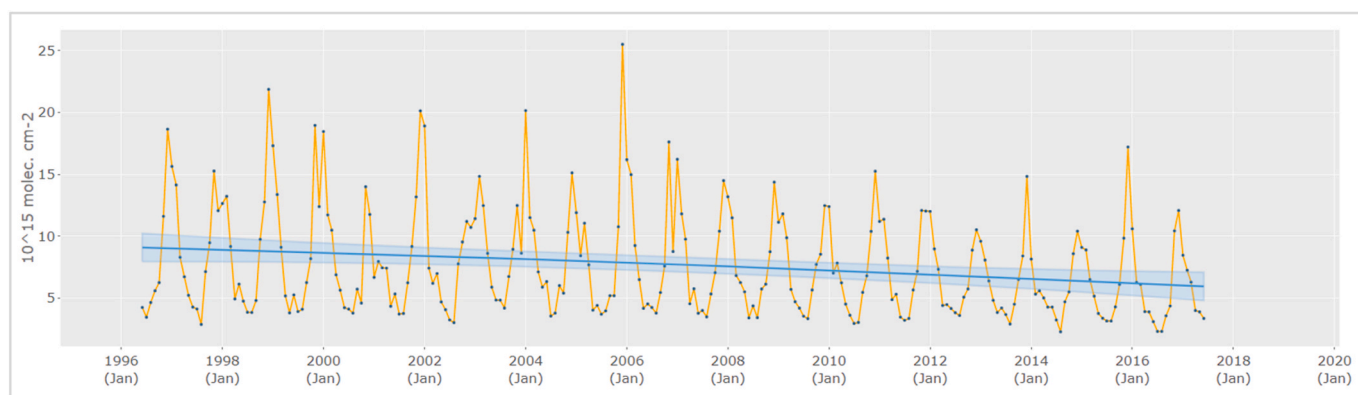

Fig. 6. Time series of the tropospheric NO_2 monthly mean column values from 1996 to 2017 based on GOME, SICAMCHY, GOME-2A and GOME-2B observations for the area of northern Italy (Latitudes: 44°–46°, Longitudes: 7°–14°). The blue curve represents a cubic spline fit indicating a long-term trend (see text for detail). (For interpretation of the references to colour in this figure legend, the reader is referred to the Web version of this article.)
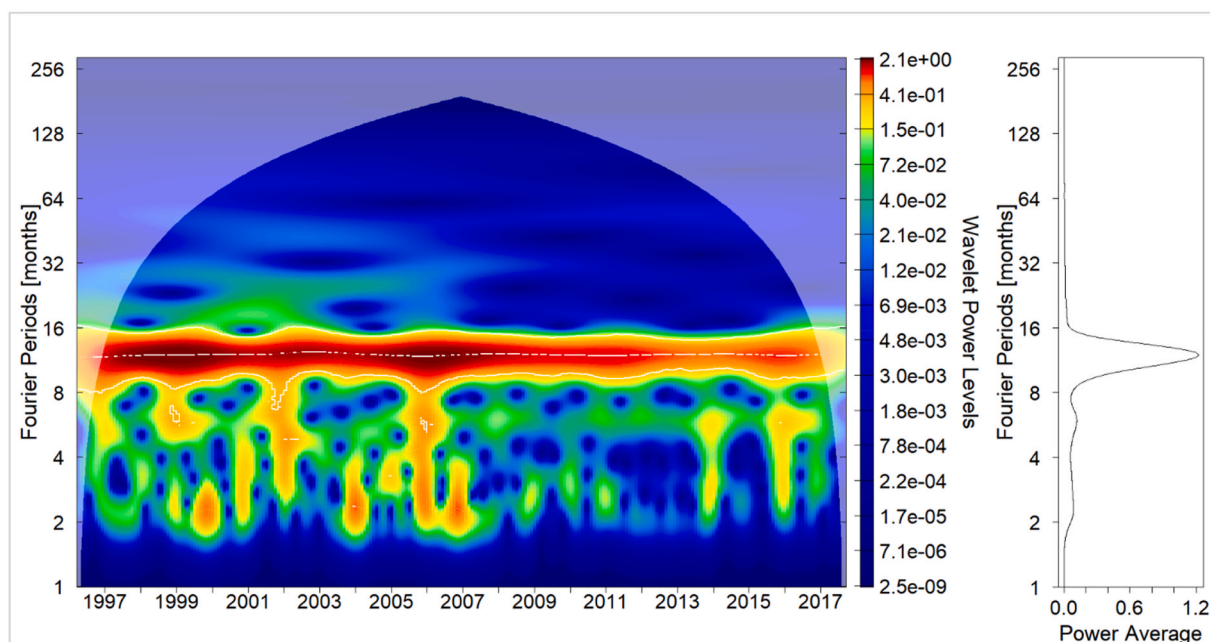
Fig. 7. Wavelet spectrogram of the monthly mean tropospheric NO$_2$ column density time series displayed in Fig. 6. The diagram in the right part of the plot shows the spectral intensity of the spectrogram averaged over the entire period.

(rate of) change where i and j are each intended to characterize different processes.

Let us first very briefly look at the typical production processes. As mentioned above, tropospheric NO$_2$ is predominantly produced in particular by fossil-fuel-combustion processes. It is therefore expected that the heating period during the cold winter months lead to an annual cycle in the temporal development of the tropospheric NO$_2$ column density (Fig. 6). Further major emitters of NO$_2$ are transport and industry. Their emissions are also not evenly distributed over the year. For example, the summer break in Italy lasts about three months which could make a further contribution to the observed annual variation. Furthermore, emission differences occur between working days, weekends, and holidays, which lead to shorter-scale variations. Other sources of NO$_2$ include lightning (Noxon, 1976), biomass burning (Seiler and Crutzen, 1980), and soil microbial activity (Williams et al., 1992). However, their shares in NO$_2$ production are negligible (e.g. Seinfeld and Pandis, 2016).

As far as the loss processes of NO$_2$ are concerned, meteorology also plays a role here in addition to the chemical degradation processes. For example, the highest precipitation rates in northern Italy are typically found in May and November (Climate-Data.ORG, 2021). This supports the occurrence of a semi-annual cycle in the tropospheric NO$_2$ column density. Typical weather changes, if associated with different precipitation intensities, also contribute to the temporal variability of tropospheric NO$_2$ column density. In order to better assess the influence of meteorology, the 10 m horizontal wind and total precipitation time series for the area of interest was examined with a wavelet analysis method. The results showed that meteorological conditions were likely not the reason for the significant decrease in NO$_2$ variability over the period 2007 to mid-2013. By comparing the three periods A, B, and C (Fig. 9) of the total precipitation and calculating the mean values (*A*: 1.04 mm, *B*: 1.22 mm, *C*: 1.26 mm) as well as the variance (*A*: $3.46*10^{-7}$, *B*: $3.73*10^{-7}$, *C*: $4.76*10^{-7}$), no significant higher total precipitation can be determined for period B. The same investigations were also carried out for the horizontal wind where period A had a mean value of 0.41 m/s, period B 0.41 m/s, and period C 0.43 m/s, as well as for the variance (A: 0.029, B: 0.035, C: 0.028). Only satellite data with a very low cloud coverage (cloud fraction <20%) were used for the TEMIS data product. This means that the influence of the precipitation has

already been weakened by this criterion.

The large-scale weather systems in the middle geographical latitudes are decisively characterized by so-called planetary waves. These planetary waves, which are a direct consequence of the Earth's rotation and the meridional pressure gradient between lower and higher latitudes, influence the temporal sequence of high- and low-pressure systems (a comprehensive description of the planetary waves is given, for example, in Andrews, 2010; Petoukhov et al., 2013; Screen and Simmonds, 2014, and the references given therein). The typical periods of these waves range from a few days up to several weeks. In this respect, it is to be expected that in principle these signatures are also reflected to some extent in the spectrograms (Figs. 7 and 8).

Finally, transport processes can also influence the temporal variability of the tropospheric NO$_2$ column density. Thus, air masses rich or poor in NO$_2$ can be transported into our target area to a certain extent. In addition, there is broad agreement that tropospheric NO$_2$ levels can also be influenced by downward transport from the stratosphere. In the mid-latitudes, so-called tropopause folds, cold air drops and streamers are known to be particularly effective processes for this. These processes are essentially episodic and thus may also contribute to the temporal fluctuations of the tropospheric NO$_2$ column density shown in Figs. 7 and 8. However, their estimated contribution to the tropospheric NO$_2$ is regarded to be at least two to three orders of magnitudes lower than the aforementioned emission from fossil-fuel-combustion (e.g. Seinfeld and Pandis, 2016).

Fig. 11 presents the amplitudes for the annual oscillation of the tropospheric column NO$_2$ density. The strength of the seasonal oscillations varies from year to year, which underlines the non-stationarity of the data series already mentioned in section 3. It also appears as if the amplitudes turn out systematically higher almost every two years (1996–2007). This could offer further opportunities for research on the impact of the so-called quasi-biennial oscillation (QBO) which is created in the equatorial stratosphere due to a wind change in an almost two-year cycle (Naujokat and Marquardt, 1992). This aspect is beyond of the scope of our paper, furthermore these fluctuations are comparatively small and play only a minor role for the study presented here.

During winter the height of the boundary layer is often lower than during summer. As a consequence, the removal of NO$_2$-rich air masses by the air flow is less efficient in winter. We assume that this can explain
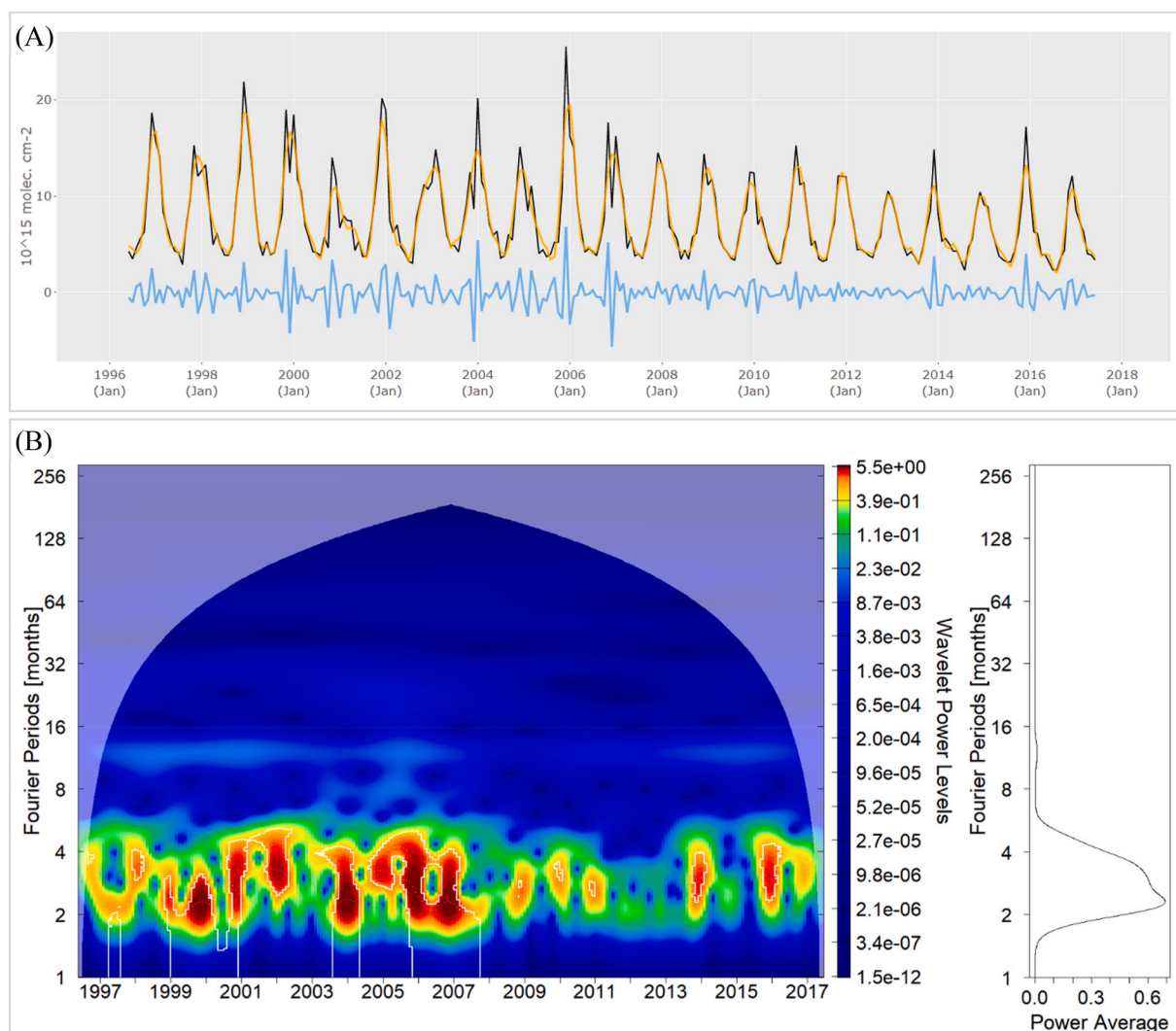
Fig. 8. (A) Harmonic Analysis which presents the fit of the annual and the semi-annual cycle (orange) to the time series of the NO$_2$ tropospheric column densities (black). The residues form the blue curve. (B) Wavelet spectrogram of the residues. (For interpretation of the references to colour in this figure legend, the reader is referred to the Web version of this article.)

– at least in part – the systematically higher intensities in the spectro-grams during winter (Figs. 7 and 8). Pernigotti et al. (2012) also mention the frequently lower wind regimes during winter in the Po valley. A so-called cold air pool (CAP) can be formed in the Po valley because of the topographical situation in northern Italy and due to lower solar radiation in wintertime, the accumulation of pollutants can be supported by affecting convective mixing and dispersion (Holmes et al. 2015). This could be one explanation why the NO$_2$ pollutants accumulate better over a certain area during winter and therefore cause higher NO$_2$ concentrations. With regard to the wind regimes, further studies on the urban boundary layer (UBL) could also provide more information about the situation for the area of interest in this paper. Referring to Wang et al. (2019) who analyzed the structure of the UBL over the urban Beijing area concluded that low surface temperature, weak wind regimes, a high relative humidity, and temperature inversion had an impact on the observed particulate matter 2.5 (PM 2.5) air pollution events. Such effects on NO$_2$ were not closer analyzed for the area of interest in this paper but would offer potential for future studies.

Temporal fluctuations (weekly, monthly, yearly) of the tropospheric NO$_2$ column density over the entire spectral range are expected due to the various production, loss, and transport processes (equation (6)). This expectation is fulfilled by the spectrograms presented in Figs. 7 and 8. For the sake of completeness, it should be noted that due to the temporal

resolution of the time series of tropospheric NO$_2$ column density, temporal variations shall only be considered above approximately two months according to the Nyquist-Shannon criterion. Furthermore, we provisionally assume that the variabilities found are essentially due to fossil-fuel-combustion processes.

5.3. Gross national product and NO$_2$ variability

Fig. 8 shows the spectrogram of the tropospheric NO$_2$ column density time series adjusted for the annual and semi-annual variation. As outline above we tentatively assume that the remaining significant spectral intensities can essentially be attributed to emissions from traffic, and industry. The fluctuations in tropospheric NO$_2$ column density caused by the diversity of these emissions and their decomposition are characterized by a spectral quasi-continuum. This is shown in the right part of Fig. 8 as averaged spectral intensity over the entire time period as a function of the oscillation period.

The spectrogram (Fig. 8) shows that in the period between about 2008 and mid-2013 the spectral intensities are significantly reduced. In fact, the intensities are systematically about one order of magnitude lower than in the periods from 1996 to 2007 and from mid-2013 to 2017 (Fig. 9). These finding suggests that this behavior can be attributed to a reduction in emissions from transport and industry. Fig. 5 shows a deep
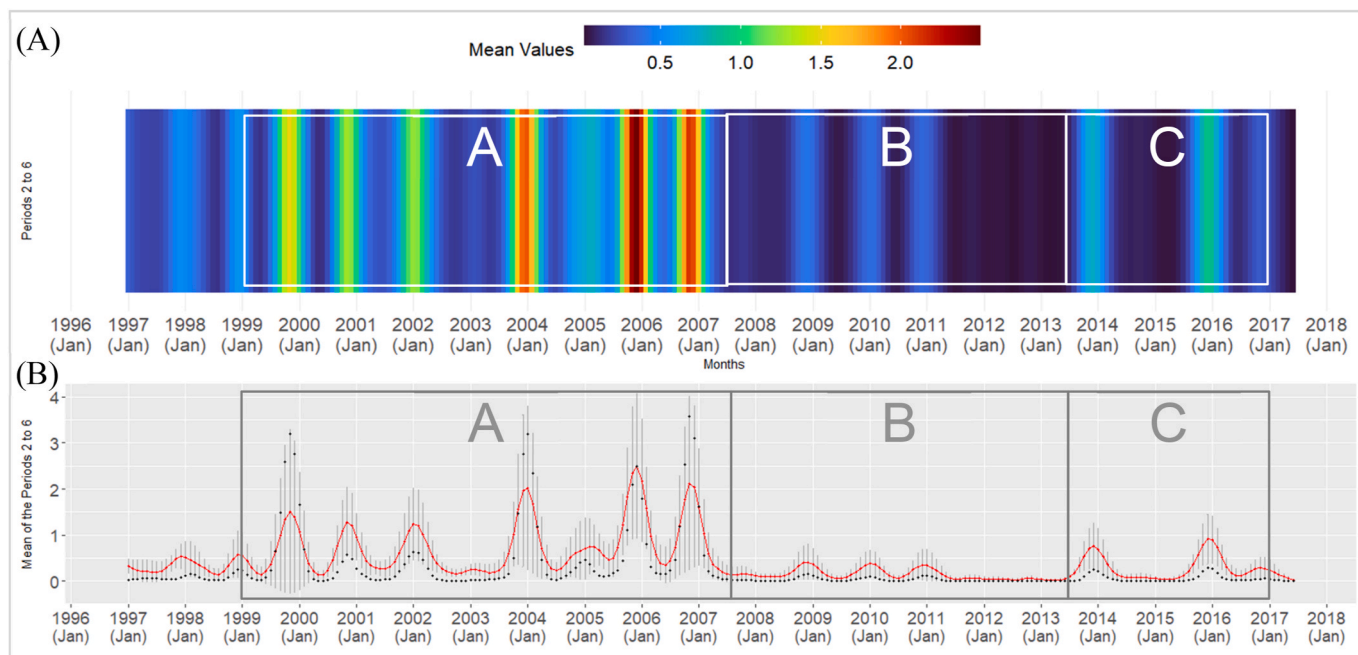
Fig. 9. (A) Calculated mean values of the wavelet analysis (Fig. 8) for the periods two to six. (B) red line presents the mean values of the wavelet analysis (Fig. 8) for the periods between two to six; grey bars represent the standard deviation based on the mean values; black dots show the variation. (For interpretation of the references to colour in this figure legend, the reader is referred to the Web version of this article.)
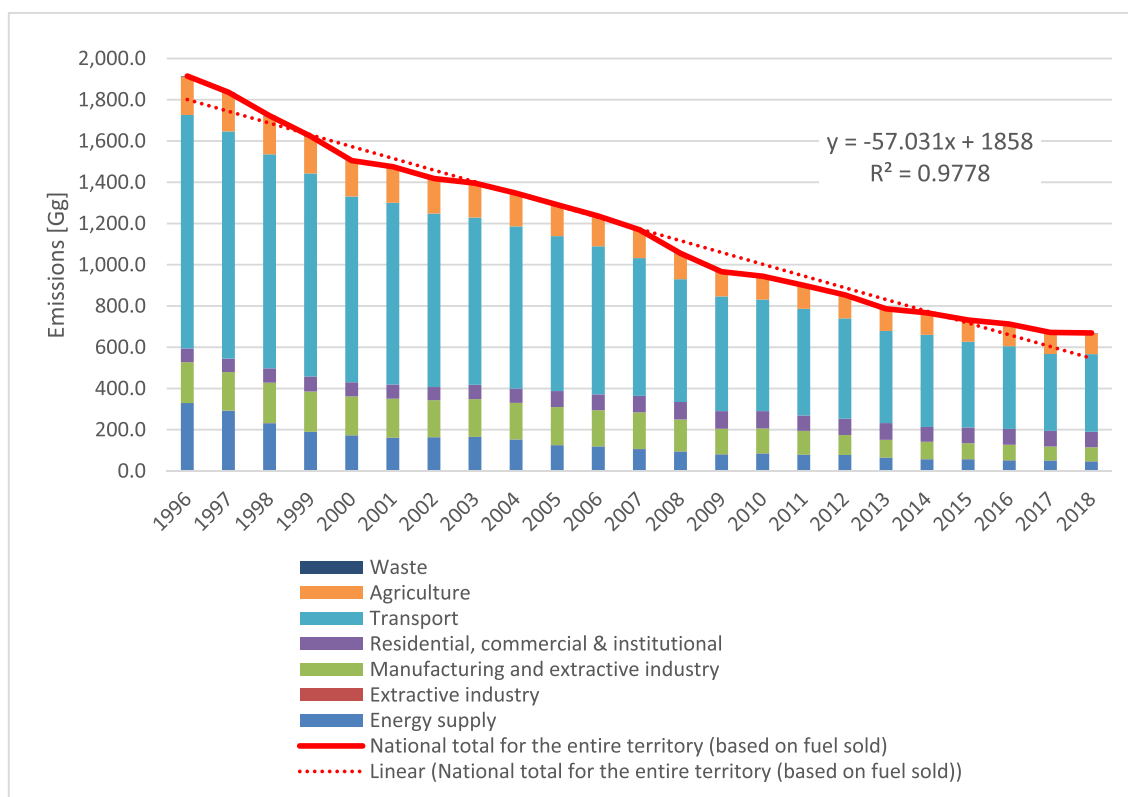

Fig. 10. Emission Data from the National Emission reduction Commitments Directive [NECD] of NOx for Italy; Bar diagram presents different sectors; Red line shows the total amount and the dotted red line presents the linear trend between 1996 and 2018 in Italy (Fig. taken from: EEAa, 2021). (For interpretation of the references to colour in this figure legend, the reader is referred to the Web version of this article.)

decline in Italy's economic performance from 2008 onwards, with GDP falling by about 6% within a year. This collapse marks the period of the global financial crisis of 2008. It then recovers only comparatively

slightly by about 1.5% until 2011 and then falls again by almost another 5% in the years until 2013 to a new low. At the beginning of the global financial crisis in 2008, Italy's public debt was around 100%. This made
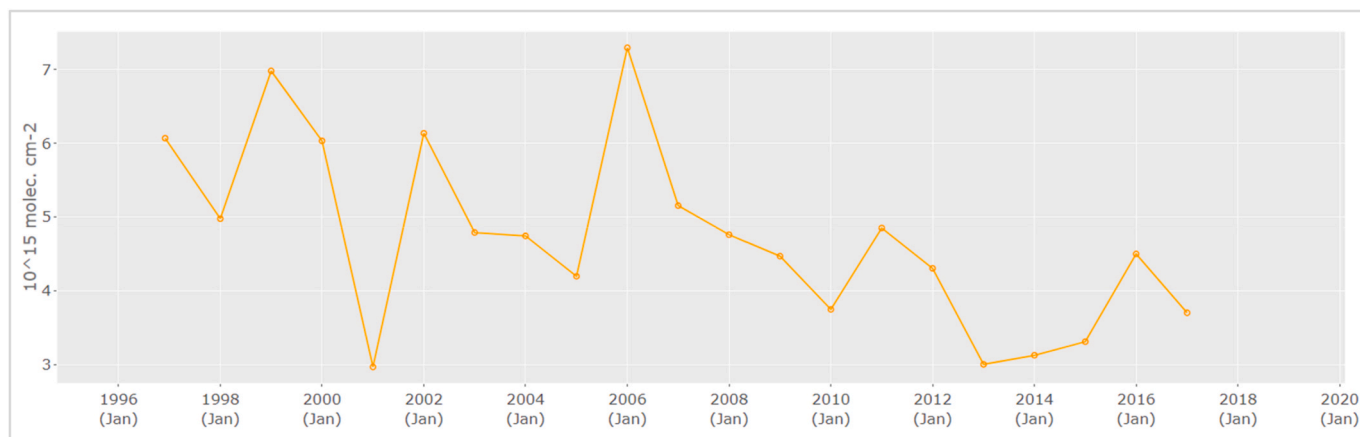
Fig. 11. Amplitudes of the annual cycle of the tropospheric NO_2 column density.

it particularly difficult to pay off maturing loans from investors, who were also reluctant to invest further. As a result, Italian industrial production shrank significantly. While other countries (Fig. 5) generated growth again, this was no longer possible in Italy to a comparable extent. Since 2014, Italy's economy has been growing steadily again. In 2021 the country is approximately back at the level it was in the year 2000. However, this does not yet consider the very significant economic collapse caused by the COVID-19 pandemic in 2020, which is beyond the scope of this paper. The spectrogram of the time series of the tropospheric NO_2 column density (Fig. 8) shows Italy's economic weakness from 2008 to 2014 with a significant reduction in spectral intensity. We therefore conclude that temporal variations in economic performance are particularly evident in the temporal fluctuations of tropospheric NO_2 column density. Furthermore, we suggest that there might be a causal relationship between economic activity (represented by GDP) on the one hand and the variability of tropospheric NO_2 column densities on the other.

In the time interval from mid-2007 to mid-2013, Italy's GDP decreased by around 11.7% (Fig. 5). For the same time interval, our analyses (Fig. 8) show a reduction in integrated spectral intensity of the fluctuations of the tropospheric NO_2 column density in the range from two to six months of about 81% compared to the preceding time interval from 1999 to mid-2007, and of about 52% compared to the succeeding time interval from mid-2013 to the end of 2016.

6. Summary and conclusion

This paper explores whether there is a possible link between the development of economic activity and the temporal fluctuations of the tropospheric NO_2 column density as measured by satellite. We chose the Po valley in northern Italy as a test region. In our opinion, it should be possible to reliably prove a connection – if any – due to the special orography and the high level of industrialization. We therefore compared the Italian GDP development over time which is with a time series of satellite-based monthly mean tropospheric NO_2 column density measurements for northern Italy between 1996 and 2017. It should be noted that the majority of the Italian GDP is generated in northern Italy.

To produce a consistent and complete time series of tropospheric NO_2 column density for the period from 1996 to 2017, a self-consistent satellite data product from TEMIS is used. The product includes tropospheric measurements from ERS-2/GOME, Envisat/SCIAMACHY, MetOp-A/GOME-2, and MetOp-B/GOME-2 each overflying the region at approximately the same local time.

- As a first result we find a long-term decrease of the temporal development of the tropospheric NO_2 column density of about 35%

since 1996 which is in good agreement with other work and trends derived from ground-based station measurements.

- A dominant annual cycle as well as a semi-annual cycle is found to be superimposed on this long-term development. It is also interesting that a quasi-two-year cycle can be assumed in the first half of the time series. This signal will be greatly weakened from 2007 onwards.

In order to study the shorter-term fluctuations in the tropospheric NO_2 column density time series we removed both, the annual and the semi-annual cycle from the data. To account for the transient nature of the time series, these seasonal cycles were adjusted separately for each year using the least squares harmonic analysis approach and subtracted from the data set. The time series of the residues generated by subtracting the annual, and semi-annual cycle from the original NO_2 time series contains the fluctuations in tropospheric NO_2 column densities. This new time series is highly non-stationary in the statistical sense. The fluctuations were therefore analyzed with the wavelet-technique using a Morlet-wavelet as the mother wavelet function.

- The fluctuations of the tropospheric NO_2 column density in the time range of about two to six months (Fig. 8) are a composition of various production, loss and transport processes for NO_2. The spectrogram exhibits remarkably low spectral variability between mid-2007 and mid-2013 for the periods two to six months (Fig. 9 period B). Compared to previous (Fig. 9 period A) and subsequent years (Fig. 9 period C), intensities are reduced by about 81% and 52% during the period of crises (Fig. 9 period B).
- The comparison with the temporal course of the GDP shows that the period of systematically reduced spectral intensity in the tropospheric NO_2 column densities coincides strikingly well with the period of the global financial crisis in 2008 which was then followed by a decline in foreign investment until about 2014. Within these years Italy's GDP decreased by about 11.7%. This shows – as a major result of this work – that fluctuations in tropospheric NO_2 column density are sensitive to changes in economic growth.

We therefore suggest that the use of globally available NO_2 data sets and their analysis with respect to fluctuations should in principle allow changes in economic activity to be recorded in any region of the Earth with remarkable sensitivity. Such an indicator could help to monitor not only global economic development, but possibly also the transition in regions between different levels of economic development (primary, secondary, and tertiary economic sector). However, this still requires further work.

The strength of satellite-based observations lies on the one hand in the global coverage and on the other hand in the self-consistency of the measurements (uniform standard). However, they only give us

information about the tropospheric NO_2 column density. Information on ground-level air quality is not available and transport effects are masked to a certain extent. Present-day satellite overpasses usually occur only at a specific time of the day. Therefore, the daily cycle of NO_2 (including the effect of traffic rush hours etc.) cannot be analyzed by using such satellite data only. The synergistic use of satellite-based and ground-based measurements is thus an avenue for improvement. Further research on a correlation between the growth rate and NO_2 pollution should also be considered by disaggregating economic sectors (primary, secondary, and tertiary sectors) as well as comparing the NO_2 variability tied to consumer spending.

CRediT authorship contribution statement

Renée Bichler: Writing – original draft, (equal), Writing – review & editing, (lead), Data curation, Software, Programming, Formal analysis, Visualization. **Michael Bittner:** Conceptualization, Writing – original draft, (equal), Writing – review & editing, (support), Supervision, Methodology.

Declaration of competing interest

The authors declare that they have no known competing financial interests or personal relationships that could have appeared to influence the work reported in this paper.

Acknowledgement

References

Andrews, D.G., 2010. An Introduction to Atmospheric Physics, second ed. Cambridge University Press.

Bigi, A., Ghermandi, G., Harrison, R.M., 2012. Analysis of the air pollution climate at a background site in the Po valley. J. Environ. Monit. 14, 552–563. https://doi.org/10.1039/c1em10728c.

Bittner, M., Offermann, D., Bugaeva, I.V., Kokin, G.A., Koshelkov, J.P., Krivolutsky, A., Tarasenko, D.A., Gil-Ojeda, M., Hauchecorne, A., Lübken, F.-J., de la Morena, B.A., Mourier, A., Nakane, H., Oyama, K.I., Schmidlin, F.J., Soule, I., Thomas, L., Tsuda, T., 1994. Long period/large scale oscillations of temperature during the DYANA campaign. J. Atmos. Terr. Phys. 56, 1675–1700. https://doi.org/10.1016/0021-9169(94)90004-3.

Bittner, M., Offermann, D., Graef, H.H., 2000. Mesopause temperature variability above a midlatitude station in Europe. J. Geophys. Res. 105 (D2), 2045–2058.

Bo, M., Salizzioni, P., Pognant, F., Mezzalama, R., Clerico, M., 2020. A combined citizen science – modelling approach for NO_2 assessment in Torino urban agglomeration. Atmosphere 11, 721. https://doi.org/10.3390/atmos11070721.

Boersma, K.F., Eskes, H.J., Brinksma, E.J., 2004. Error analysis for tropospheric NO_2 retrieval from space. J. Geophys. Res. 109, D04311. https://doi.org/10.1029/2003JD003962.

Boersma, K.F., 2008. Monthly mean tropospheric NO_2 datafiles (TOMS format). Online. https://d37onar3vnbj2y.cloudfront.net/static/docs/README_TOMSASCII.pdf. (Accessed 14 December 2020).

Boersma, K.F., van Geffen, J., Eskes, H., van der, A.R., 2017. Product Specification Document for the QA4ECV NO_2 ECV Precursor Product. Version 1.1. Royal Netherlands Meteorological Institute (KNMI). https://www.temis.nl/qa4ecv/no2col/QA4ECV_NO2_PSD_v1.1.compressed.pdf. (Accessed 14 December 2020).

Bovensmann, H., Burrows, J.P., Buchwitz, M., Frerick, J., Noel, S., Rozanov, V.V., Chance, K.V., Goede, A.H.P., 1999. Sciamachy – mission objectives and measurement modes. J. Atmos. Sci. 56, 127–150.

Brasseur, G., Solomon, S., 1986. Aeronomy of the Middle Atmosphere, second ed. D. Reidel Publishing Company, Dordrecht, Holland.

Burrows, J.P., Hölzle, E., Goede, A., Visser, H., Fricke, W., 1995. Sciamachy – scanning imaging absorption spectrometer for atmospheric chartography. Acta Astronaut. 35, 445–451. https://doi.org/10.1016/0094-5765(94)00278-T.

Burrows, J.P., Weber, M., Buchwitz, M., Rozanov, V., Ladstaetter-Weissenmayer, A., Richter, A., Debeek, R., Hoogen, R., Bramstedt, K., Eichmann, K.-U., Eisinger, M., Perner, D., 1999. The global ozone monitoring exeriment (GOME): mission concept and first scientific results. J. Atmos. Sci. 56, 151–175.

Castellanos, P., Boersma, K.F., 2012. Reduction in nitrogen oxides over Europe driven by environmental policy and economic recession. Sci. Rep. 2, 265. https://doi.org/10.1038/srep00265.

Chui, C.K., 1992. An introduction to wavelets. Math. Comput. 60 (202), 854. https://doi.org/10.2307/2153134.

Climate-DataOrg, 2021. Klima Mailand (Italien). Daten und Graphen zum Klima und Wetter für Mailand. Online: https://de.climate-data.org/europa/italien/lombardei/mailand-1094/#climate-graph (last access: 31-Aug-2021).

Degraeuwe, B., Thunis, P., Clappier, A., Weiss, M., Lefebvre, W., Janssen, S., Vranckx, S., 2017. Impact of passenger car NOx emissions on urban NO_2 pollution – scenario analysis for 8 European cities. Atmos. Environ. 171, 330–337. https://doi.org/10.1016/j.atmosenv.2017.10.040.

Dinda, S., Coondoo, D., Pal, M., 2000. Air quality and economic growth: an empirical study. Ecol. Econ. 34, 409–423. https://doi.org/10.1016/S0921-8009(00)00179-8.

EEA, 2021. National emission reduction Commitments directive. Online. https://www.eea.europa.eu/themes/air/air-pollution-sources-1/national-emission-ceilings. (Accessed 2 June 2021).

EEAa, 2021. National Emission Ceilings Directive Emissions Data Viewer 1990-2018. Online: https://www.eea.europa.eu/data-and-maps/dashboards/necd-directive-data-viewer-3. (Accessed 1 June 2021).

Filonchyk, M., Peterson, M., 2020. Air quality in Shanghai, China, and the surrounding urban agglomeration during the COVID-19 lockdown. Journal of Geovisualization and Spatial Analysis 4, 22. https://doi.org/10.1007/s41651-020-00064-5.

Filonchyk, M., Hurynovich, V., Yan, H., 2021. Impact of COVID-19 pandemic on air pollution in Poland based on surface measurements and satellite data. Aerosol Air Qual. Res. 21 (7), 1–13. https://doi.org/10.4209/aaqr.200472, 200472.

G-Econ Project, 2009. Geographically Based Economic Data (G-Econ). Online. https://gecon.yale.edu/g-econ-project-yale-university-september-2009. (Accessed 23 June 2021).

Georgoulias, A.K., van der A, R.J., Stammes, P., Boersma, K.F., Eskes, H.J., 2019. Trends and trend reversal detection in 2 decades of tropospheric NO_2 satellite observations. Atmos. Chem. Phys. 19, 6269–6294. https://doi.org/10.5194/acp-19-6269-2019.

Grossmann, G.M., Krueger, A.B., 1995. Economic growth and the environment. Q. J. Econ. 112, 353–378. https://doi.org/10.2307/2118443.

Hersbach, H., Bell, B., Berrisford, P., Biavati, G., Horányi, A., Muñoz Sabater, J., Nicolas, J., Peubey, C., Radu, R., Rozum, I., Schepers, D., Simmons, A., Soci, C., Dee, D., Thépaut, J.-N., 2018. ERA5 Hourly Data on Single Levels from 1979 to Present. https://doi.org/10.24381/cds.adbb2d47. Copernicus Climate Change Service (C3S) Climate Data Store (CDS). (Accessed 20 June 2021).

Holmes, H.A., Sriramasamudram, J.K., Pardyjak, E.R., Whiteman, C.D., 2015. Turbulent fluxes and pollutant mixing during wintertime air pollution episodes in complex terrain, 2015 Environ. Sci. Technol. 49, 13206–13214. https://doi.org/10.1021/acs.est.5b02616.

Jiang, M., Euijune, K., Youngjin, W., 2020. The relationship between economic growth and air pollution – a regional comparison between China and South Korea. Int. J. Environ. Res. Publ. Health 17, 2761. https://doi.org/10.3390/ijerph17082761.

Le Quéré, C., Jackson, R.B., Jones, M.W., Smith, A.J.P., Abernethy, S., Andrew, R.M., De Gol, A.J., Willis, D.R., Shan, Y., Canadell, J.G., Friedlingstein, P., Creutzig, F., Peters, G.P., 2020. Temporary reduction in daily global CO_2 emissions during the COVID-19 forced confinement. Nat. Clim. Change 10, 647–653. https://doi.org/10.1038/s41558-020-0797-x.

Levy II, H., Moxim, W.J., 1999. Simulated tropospheric NOx: its evaluation, global distribution and individual source contributions. J. Geophys. Res. 104 (D21), 26279–26306.

Liu, S., Valks, P., Beirle, S., Loyola, D.G., 2021. Nitrogen dioxide decline and rebound observed by GOME-2 and TROPOMI during COVID-19 pandemic. Air Quality Atmos. Health 14, 1737–1755. https://doi.org/10.1007/s11869-021-01046-2.

Masiol, M., Agostinelli, C., Formenton, G., Tarabotti, E., Pavoni, B., 2014. Thirteen years of air pollution hourly monitoring in a large city: potential sources, trends, cycles and effects of car-free days. Sci. Total Environ. 494–495, 84–96. https://doi.org/10.1016/j.scitotenv.2014.06.122.

Munro, R., Lang, R., Klaes, D., Poli, G., Retscher, C., Lindstrot, R., Huckle, R., Lacan, A., Grzegorski, M., Holdak, A., Kokhanovsky, A., Livschitz, J., Eisinger, M., 2016. The GOME-2 instrument on the Metop series of satellites: instrument design, calibration, and level 1 data processing – an overview. Atmos. Meas. Tech. 9, 1279–1301. https://doi.org/10.5194/amt-9-1279-2016.

Naujokat, B., Marquardt, C., 1992. Die annähernd zweijährige Schwingung (QBO). Promet. Meteorologische Fortbildung 22 (2–4), 62–68.

Noxon, J.F., 1976. Atmospheric nitrogen fixation by lightning. Geophys. Res. Lett. 3, 463–465. https://doi.org/10.1029/GL003i008.

OECD, 2021. GDPVD_CAP: Gross Domestic Product Per Capita volume in USD, at constant purchasing power parities. Online. https://stats.oecd.org/Index.aspx?DataSetCode=EO104_INTERNET. (Accessed 31 March 2021).

Ortega, J.M., Rheinboldt, W.C., 1970. Iterative solution of nonlinear equations in several variables. Comput. Sci. Appl. Mathemat. University of Pittsburgh.

Pernigotti, D., Georgieva, E., Thunis, P., Bessagnet, B., 2012. Impact of meteorology on air quality modeling over the Po valley in northern Italy, 2012 Atmos. Environ. 51, 303–310. https://doi.org/10.1016/j.atmosenv.2011.12.059.

Petoukhov, V., Rahmstorf, S., Petri, S., Schellnhuber, H.J., 2013. Quasiresonant amplification of planetary waves and recent Northern Hemisphere weather extremes. Proc. Natl. Acad. Sci. U.S.A. 110 (14), 5336–5341. https://doi.org/10.1073/pnas.1222000110.

Piersanti, A., D'Elia, I., Gualtieri, M., Briganti, G., Cappelletti, A., Zanini, G., Ciancarella, L., 2021. The Italian national air pollution control programme: air quality, health impact and cost assessment. Atmosphere 12, 196. https://doi.org/10.3390/atmos12020196.

Raffaelli, K., Deserti, M., Stortini, M., Amorati, R., Vasconi, M., Giovannini, G., 2020. Improving air quality in the Po valley, Italy: some results by the LIFE-IP-PREPAIR project. Atmosphere 11, 429. https://doi.org/10.3390/atmos11040429.

Roesch, A., Schmidbauer, H., 2018. WaveletComp: Computational Wavelet Analysis. R package version 1.1 Online. https://cran.r-project.org/web/packages/WaveletComp/WaveletComp.pdf. (Accessed 22 September 2020).

Russell, A.R., Valin, L.C., Cohen, R.C., 2012. Trends in OMI NO_2 observations over the United States: effects of emission control technology and the economic recession. Atmos. Chem. Phys. 12, 12197–12209. https://doi.org/10.5194/acp-12-12197-2012.

Schaap, M., Kranenburg, R., Curier, L., Jozwicka, M., Dammers, E., Timmermans, R., 2013. Assessing the sensitivity of the OMI-NO_2 product to emission changes across Europe, 2013 Rem. Sens. 5, 4187–4208. https://doi.org/10.3390/rs5094187.

Screen, J., Simmonds, I., 2014. Amplified mid-latitude planetary waves favour particular regional weather extremes. Nat. Clim. Change 4, 704–709. https://doi.org/10.1038/nclimate2271.

Seiler, W., Crutzen, P.J., 1980. Estimates of gross and net fluxes of carbon between the biosphere and the atmosphere from biomass burning. Climatic Change 2, 207–247. https://doi.org/10.1007/BF00137988.

Seinfeld, J.H., Pandis, S.N., 2016. Atmospheric Chemistry and Physics. From Air Pollution to Climate Change, third ed. John Wiley & Sons, Inc., Hoboken, New Jersey, p. 1120.

Shah, V., Jacob, D.J., Li, K., Silvern, R.F., Zhai, S., Liu, M., Lin, J., Zhang, Q., 2020. Effect of changing NOx lifetime on the seasonality and long-term trends of satellite-observed tropospheric NO_2 columns over China. Atmos. Chem. Phys. 20, 1483–1495. https://doi.org/10.5194/acp-20-1483-2020.

Steinbrecht, W., Kubistin, D., Plass-Dülmer, C., Davies, J., Tarasick, D.W., Gathen, P., et al., 2021. COVID-19 crisis reduces free tropospheric ozone across the Northern Hemisphere. Geophys. Res. Lett. 48, e2020GL091987 https://doi.org/10.1029/2020GL091987.

Torrence, C., Compo, G.P., 1998. A practical guide to wavelet analysis. Bull. Am. Meteorol. Soc. 79 (1), 61–78. https://doi.org/10.1175/1520-0477(1998)079%3C0061:APGTWA%3E2.0.CO;2.

Velders, G.J.M., Granier, C., Portmann, R.W., Pfeilsticker, K., Wenig, M., Wagner, T., Platt, U., Richter, A., Burrows, J.P., 2001. Global tropospheric NO_2 column distributions: comparing three-dimensional model calculations with GOME measurements. J. Geophys. Res. 106 (D12), 12643–12660. https://doi.org/10.1029/2000JD900762.

Wallace, J.M., Hobbs, P.V., 2006. Atmospheric Science. An Introductory Survey, second ed. Elsevier, Academic Press, p. 483. 30 Corporate Drive, Suite 400, Burlington, MA 01803, USA and 525 B Street, Suite 1900, San Diego, California 92101-4495, USA and 84 Theobald's Road, London WC1X 8 RR, UK.

Wang, L., Liu, J., Gao, Z., Li, Y., Huang, M., Fan, S., Zhang, X., Yang, Y., Miao, S., Zou, H., Sun, Y., Chen, Y., Yang, T., 2019. Vertical observations of the atmospheric boundary layer structure over Beijing urban area during air pollution episodes. Atmos. Chem. Phys. 19, 6949–6967. https://doi.org/10.5194/acp-19-6949-2019.

Williams, E.J., Hutchinson, G.L., Fehsenfeld, F.C., 1992. NOx and N2O emissions from soil. Global Biogeochem. Cycles 6, 351–388. https://doi.org/10.1029/92GB02124.

World Bank, 2020. World Development Indicators: Structure of Output. Online: http://wdi.worldbank.org/table/4.2. (Accessed 15 September 2020).

Wuest, S., Bittner, M., 2006. Non-linear resonant wave-wave interaction (triad): case studies based on rocket data and first application to satellite data. J. Atmos. Sol. Terr. Phys. 68 (9), 959–976. https://doi.org/10.1016/j.jastp.2005.11.011.